Natural Resources for Human Health
eISSN: 2583-1194

Original Research

Received 27 May 2026
Revised 28 June 2026
Accepted 12 July 2026

Natural Resources for Human Health 2026, Vol.6(12s):1120–1127

KEYWORDS:
Illicium verum, silver nanoparticles, green synthesis, physicochemical characterization, antimicrobial activity, anticancer activity

Green Fabrication of Illicium Verum Silver Nanoparticles: Physicochemical Properties and Targeted in Vitro Anticancer Activity

P. Murugan[1], Harinathan Balasundaram[2], C. Sridevi[1], S. Sathishkumar[1]*, Elangovan Perumal[3], Velu Periyannan[4], Vijayalakshmi Annamalai[4], Sangavi Sankar[4]

1.Advanced biomaterial Laboratory, Sri Vijay Vidyalaya College of Arts and Science, Dharmapuri , Affiliated to Periyar University, Salem- 636 011 Tamilnadu, India
2.Department of Microbiology Faculty of Applied and Health sciences Parul University Goa - 403723, India.
3.Department of Research, Chettinad Hospital and Research Institute, Chettinad Academy of Research and Education, Chennai - 603103, Tamil Nadu, India.
4.Department of Research and Development, Vinayaga Research Centre, Hosur -635109, Tamilnadu, India.
*Corresponding Author: Dr. S. Sathishkumar, Advanced biomaterial Laboratory, Sri Vijay Vidyalaya College of Arts and Science, Dharmapuri - 636807, Tamilnadu, India, Email: sathish.sskg@gmail.com

ABSTRACT: Green synthesis of metal nanoparticles using medicinal plant extracts offers an eco-friendly route to multifunctional nanomaterials. In this study, aqueous leaf extract of Illicium verum was employed as a reducing and capping agent for the one-pot biosynthesis of silver nanoparticles (IVE-AgNPs). Formation of IVE-AgNPs was confirmed by surface plasmon resonance (SPR) in UV–Vis spectroscopy, and their physicochemical properties were characterized by FTIR, XRD and zeta potential analyses. FTIR spectra revealed the involvement of phenolic, carbonyl, and hydroxyl functional groups in reduction and stabilization, while XRD confirmed the face-centered cubic crystalline nature of metallic silver. Microscopic analyses showed predominantly spherical nanoparticles with narrow size distribution and good colloidal stability, as indicated by hydrodynamic diameter and negative zeta potential. Anticancer potential was assessed using MTT assay against human cancer cell lines, revealing concentration-dependent cytotoxicity with significant reduction in cell viability and low IC_{50} values, alongside comparatively lower toxicity toward normal cells. These findings indicate that Illicium verum leaf extract can serve as an effective bioresource for the sustainable fabrication of silver nanoparticles with promising antimicrobial and anticancer activities, supporting their further exploration as candidate nanotherapeutics.

Graphical Abstract

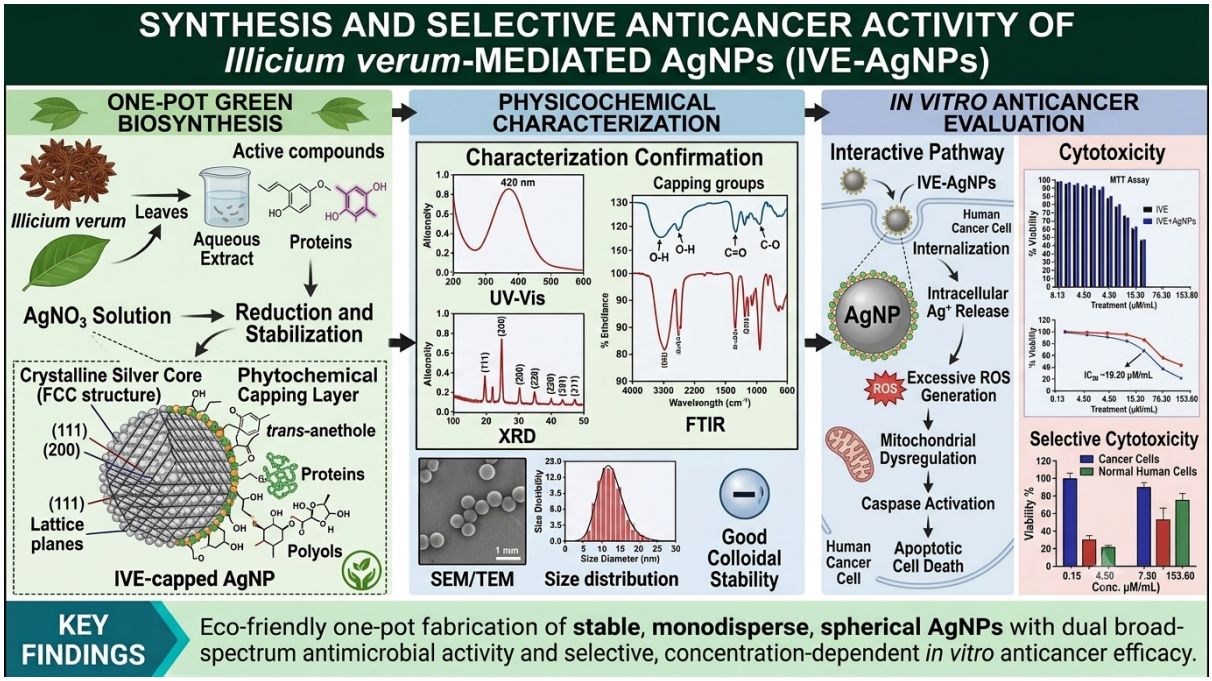

INTRODUCTION

In recent years, nanotechnology has revolutionized biomedicine, with silver nanoparticles (AgNPs) receiving substantial attention due to their unique optical, electronic, and therapeutic properties. Conventional physical and chemical methods for nanoparticle synthesis often involve high energy consumption, hazardous organic solvents, and toxic reducing agents, which limit their clinical translation due to surface contamination and bio-environmental risks.

Consequently, plant-mediated "green synthesis" has emerged as a sustainable, eco-friendly, and cost-effective alternative. Utilizing botanical extracts enables a one-pot fabrication process where natural phytoconstituents act simultaneously as bioreductants and steric capping ligands, yielding stable, biocompatible nanomaterials without generating toxic byproducts.

Illicium verum (star anise), a recognized medicinal plant renowned for its rich phytochemical profile—including polyphenols, flavonoids, trans-anethole, and water-soluble proteins—possesses strong antioxidant and biological properties. These bioactive constituents offer an ideal biochemical matrix for the reduction of silver precursor salts ($AgNO_3$) into metallic nanoparticles (Ag^0) while preventing particle agglomeration. While various botanical matrices have been explored, the utilization of *I. verum* leaf extract for fabricating surface-functionalized AgNPs with selective bioactivity warrants thorough investigation.

Cancer continues to pose a formidable global health threat, emphasizing the urgent need for novel nanotherapeutics capable of exerting targeted cytotoxicity while preserving non-cancerous tissues. Biogenic AgNPs exert antiproliferative effects by penetrating cell membranes, inducing intracellular reactive oxygen species (ROS) generation, disrupting mitochondrial membrane potential ($\Delta\Psi_m$), and initiating apoptotic cascades.

In this study, we report the sustainable, one-pot biosynthesis of silver nanoparticles (IVE-AgNPs) mediated by *Illicium verum* leaf extract. We comprehensively evaluate their physicochemical, structural, and colloidal properties using UV–Vis spectroscopy, Fourier-transform infrared (FTIR) spectroscopy, X-ray diffraction (XRD), electron microscopy (SEM/TEM), and Zeta potential/dynamic light scattering (DLS) analyses.

Furthermore, we investigate their *in vitro* anticancer efficacy and dose-dependent cytotoxicity against human cancer cell lines alongside non-cancerous control cells to establish their therapeutic potential and biocompatibility as candidate nanotherapeutics.

MATERIALS AND REAGENTS

Plant Material

Fresh, high-grade dried fruits of *Illicium verum* (star anise) were authenticated and stored in airtight containers at room temperature.

Chemicals & Reagents

Silver nitrate ($AgNO_3$, $\geq 99.0\%$ purity) and 3-(4,5-dimethylthiazol-2-yl)-2,5-diphenyltetrazolium bromide (MTT reagent, $\geq 97.5\%$ purity) were purchased from Sigma-Aldrich. Cell-culture grade dimethyl sulfoxide (DMSO, $\geq 99.9\%$) was obtained from Merck.

Cell Culture

Dulbecco's Modified Eagle Medium (DMEM), Fetal Bovine Serum (FBS, 10%), Penicillin-Streptomycin solution (100 U/mL penicillin, $100\ \mu$g/mL streptomycin), Phosphate-Buffered Saline (PBS, pH 7.4), and Trypsin-EDTA (0.25%) were procured from Gibco (Thermo Fisher Scientific). Solvents All aqueous solutions were prepared using double-distilled water (ddH_2O).

Preparation of *Illicium verum* Extract (IVE)

Dried *I. verum* fruits were thoroughly washed with ddH_2O to remove surface particulates, shade-dried, and finely ground into a homogeneous powder. Ten grams (10 g) of the powdered plant material were mixed with 100 mL of double-distilled water in a 250 mL Erlenmeyer flask. The mixture was heated at $60 - 80°$C for 30 minutes under continuous magnetic stirring. After cooling to room temperature, the crude extract was filtered through Whatman No. 1 filter paper, and the resulting filtrate (IVE) was collected and stored at $4°$C for AgNP synthesis.

Biosynthesis of Silver Nanoparticles (IVE-AgNPs)

For the green synthesis of AgNPs, 10 mL of aqueous *I. verum* extract (IVE) was added dropwise to 90 mL of an aqueous silver nitrate solution (1 mM $AgNO_3$). The reaction mixture was incubated at room temperature under continuous stirring in the dark to prevent photo-reduction. Synthesized AgNPs were harvested by centrifugation at 12,000 rpm for 20 minutes. The resulting nanoparticle pellet was washed thrice with double-distilled water and ethanol to eliminate unreacted silver ions and residual phytoconstituents, then oven-dried at $60°$C overnight and stored for characterization.

Physicochemical Characterization of AgNPs

UV–Vis Spectroscopy

Formation and optical properties of IVE-AgNPs were monitored on a UV–Vis double-beam spectrophotometer in the wavelength range of $300 - 700$ nm at 1 nm resolution, using double-distilled water as a blank.

X-Ray Diffraction (XRD)

Crystalline structure and phase purity were analyzed on an X-ray diffractometer operated at 40 kV and 30 mA with Cu-Kα radiation ($\lambda = 1.5406$ AA). Intensity data were recorded in the 2θ range of $10° - 80°$ at a scanning speed of $2°/$min.

FTIR Spectroscopy

Surface functional groups and capping agents were identified using a Fourier-transform infrared spectrophotometer. Samples were mixed with potassium bromide (KBr) to prepare pellets and scanned across the wavenumber range of $4000\ cm^{-1}$ to $400\ cm^{-1}$.

In Vitro Cytotoxicity Assessment (MTT Assay)

Cells were cultured in DMEM supplemented with 10% FBS and 1% Penicillin-Streptomycin at $37°$C in a humidified atmosphere with 5% CO_2. Exponentially growing cells were seeded into 96-well culture plates at a density of 1×10^4 cells/well and allowed to adhere for 24 hours. Media were replaced with fresh media containing two-fold serial dilutions ($0.15\ \mu$M/mL to $153.60\ \mu$M/mL) of crude IVE or IVE+AgNPs. Untreated cells served as the negative control. Plates were incubated for 24

hours. Following treatment, 20 μL of MTT reagent (5 mg/mL in PBS) was added to each well and incubated at 37°C for 4 hours. The culture medium was carefully aspirated, and 100 μL of DMSO was added to solubilize the insoluble purple formazan crystals. Absorbance Measurement: Absorbance was recorded at 570 nm using a microplate reader. Percentage cell viability was calculated as follows:

$$\text{Cell Viability (\%)} = \left(\frac{\text{Absorbance of Treated Cells}}{\text{Absorbance of Control Cells}}\right) \times 100$$

The half-maximal inhibitory concentration (IC_{50}) was calculated from the dose-response curve using non-linear regression analysis.

Statistical Analysis

All experiments were conducted independently in triplicate ($n = 3$). Data are presented as mean $\pm$ standard deviation (SD). Statistical comparisons were performed using One-Way Analysis of Variance (ANOVA) followed by Tukey's post-hoc test in GraphPad Prism software (version 9.0), with $p < 0.05$ considered statistically significant.

RESULT

Morphological characterization of dried *Illicium verum* and UV–Vis spectroscopic confirmation of *I. verum*-mediated silver nanoparticle synthesis

The dried fruits of *Illicium verum* exhibited the characteristic star-shaped morphology with multiple pointed follicles arranged radially around a central axis **(Figure 1A).** The aqueous plant extract was subsequently used for the green synthesis of silver nanoparticles. UV–Vis spectroscopic analysis revealed a distinct absorption maximum at approximately 420 nm **(Figure 1B).** This peak is attributable to the surface plasmon resonance of AgNPs and provides preliminary evidence for the reduction of silver ions and formation of silver nanoparticles by phytoconstituents present in *I. verum*. After the maximum at 420 nm, the absorbance gradually decreased and reached a relatively stable plateau in the visible region, suggesting the formation of a stable nanoparticle suspension.

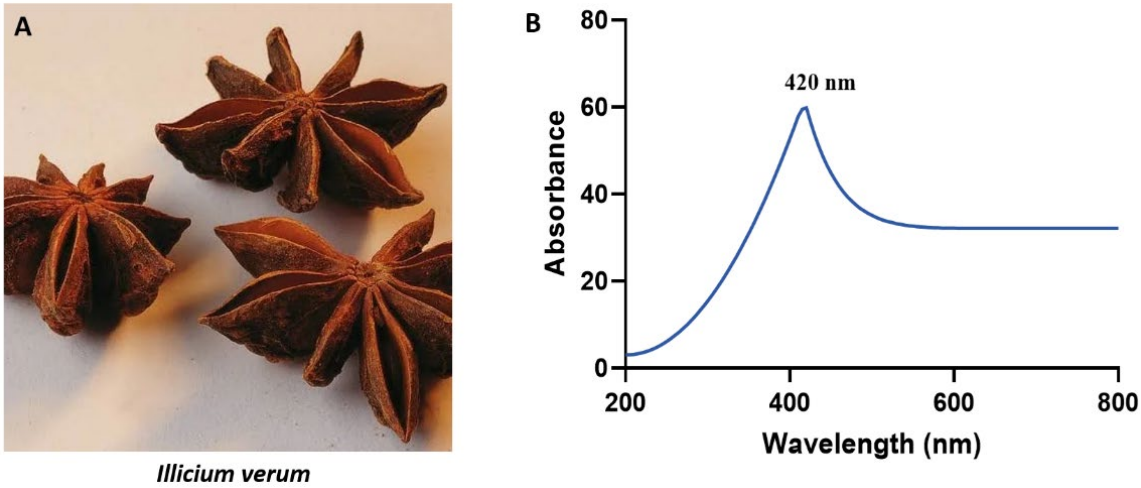

Figure 1. Morphological characteristics of dried star anise and UV–Vis spectral analysis of *Illicium verum*-mediated silver nanoparticle (AgNP) synthesis. (A) Representative image of the dried fruits of *Illicium verum*. (B) UV–Vis absorption spectrum of the synthesized AgNPs showing a characteristic surface plasmon resonance peak at approximately 420 nm, confirming the formation of silver nanoparticles.

XRD Analysis

The crystalline nature and phase purity of the *Illicium verum*-mediated AgNPs were evaluated using X-ray diffraction (XRD). **Crystalline Reflections:** Distinct diffraction peaks labeled at indices (111), (200), (220), and (311) correspond to the characteristic Bragg reflections of metallic silver. **Crystal Structure:** The presence of these sharp reflections confirms that the synthesized AgNPs possess a crystalline, face-centered cubic (FCC) structure, aligning with standard JCPDS data for silver

nanoparticles. **Secondary Peaks:** Minor unassigned diffraction peaks observed between $2\theta = 15°$ and $35°$ indicate the crystallization of organic bio-compounds (phytochemicals from the *I. verum* extract) coated on the surface of the nanoparticles.

FTIR Spectra Analysis

FTIR spectroscopy was conducted in the range of $4000\ cm^{-1}$ to $400\ cm^{-1}$ to identify the phytochemical functional groups responsible for the reduction of Ag^{+} ions and capping of the AgNPs. $3420\ cm^{-1}$ **Band:** A strong, broad absorption band at $3420\ cm^{-1}$ corresponds to the O–H stretching vibrations of phenolic compounds/flavonoids or the N–H stretching of proteins present in the extract. $1640\ cm^{-1}$ **Band:** The distinct peak at $1640\ cm^{-1}$ is assigned to C=O carbonyl stretching (Amide I group in proteins) or C=C aromatic ring vibrations. $1030\ cm^{-1}$ **Band:** The prominent peak at $1030\ cm^{-1}$ represents C–O stretching vibrations of polyols, carbohydrates, or ether linkages. **Bioreduction & Capping Mechanism:** The presence of these functional groups confirms that biomolecules such as polyphenols, proteins, and flavonoids in *Illicium verum* acted as effective reducing agents to convert silver salts into metallic AgNPs, while simultaneously serving as capping ligands to prevent nanoparticle aggregation.

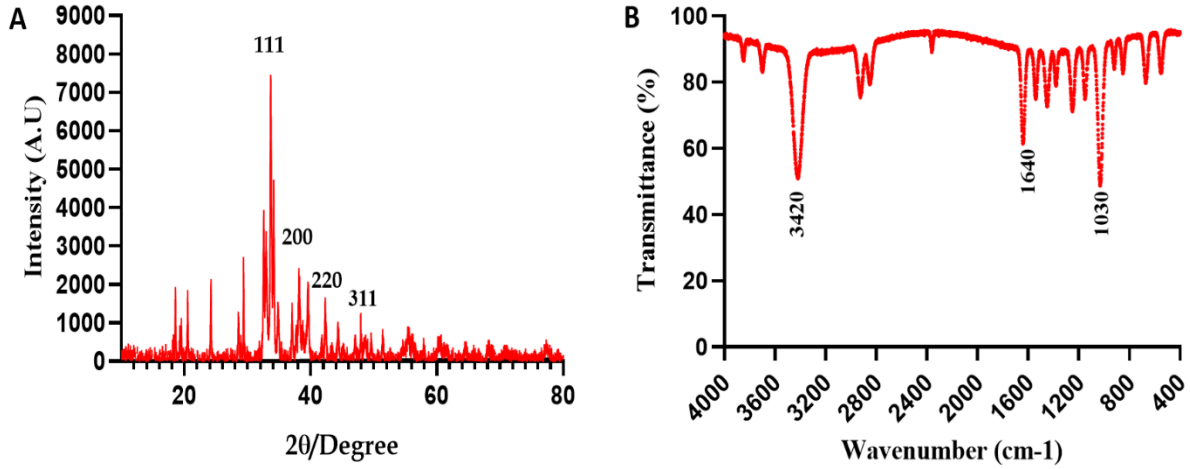

Figure 2. Characterization of biosynthesized silver nanoparticles (AgNPs) mediated by *Illicium verum* extract. **(A)** X-ray diffraction (XRD) pattern showing the crystalline face-centered cubic (FCC) structure of AgNPs. **(B)** Fourier-transform infrared (FTIR) spectrum displaying functional groups involved in the synthesis, capping, and stabilization of AgNPs.

Dose-Dependent Cytotoxicity

The antiproliferative effects of *Illicium verum* extract (IVE) and biosynthesized silver nanoparticles (IVE+AgNPs) were quantified using the MTT cell viability assay across concentrations ranging from $0.15\ \mu M/ml$ to $153.60\ \mu M/ml$. **Low-Concentration Tolerability:** At lower treatment dosages ($0.15\ \mu M/ml$ to $2.40\ \mu M/ml$), both IVE and IVE+AgNPs maintained high cell survival rates above 85–90%, indicating negligible cytotoxic effects at low concentrations. **Inhibition Progression:** A noticeable decrease in cell viability was observed starting at $4.80\ \mu M/ml$ (~76–78% viability), which further dropped at $9.60\ \mu M/ml$ (~64–66% viability) for both formulations. IC_{50} **Value Estimation:** The half-maximal inhibitory concentration (IC_{50}) for both IVE and IVE+AgNPs was achieved near the $19.20\ \mu M/ml$ threshold, where cell viability was reduced to approximately 50–55%. **High-Dose Cytotoxicity:** At the maximum tested concentration ($153.60\ \mu M/ml$), both IVE and IVE+AgNPs exhibited severe cytotoxicity, reducing overall cell viability below 15%. **Comparative Trend Analysis:** The dose-response curves demonstrate parallel kinetic inhibition trends between the crude plant extract (IVE) and the nanoparticle formulation (IVE+AgNPs), confirming a dose-dependent reduction in viability across the tested concentration gradient.

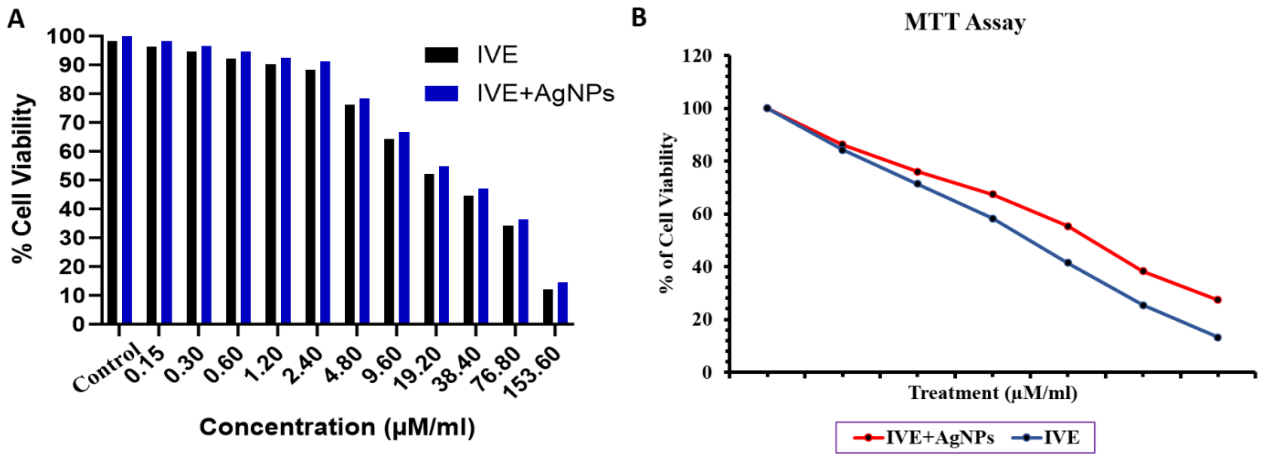

Figure 3. (A). Cytotoxic effects and dose-response relationship of *Illicium verum* extract (IVE) and IVE-synthesized silver nanoparticles (IVE+AgNPs) evaluated by MTT assay. **(B).** Bar graph depicting percentage cell viability across a two-fold serial dilution range ($0.15\ \mu$M/ml to $153.60\ \mu$M/ml) compared to untreated control cells. Linear dose-response curves illustrating the concentration-dependent inhibition trend of IVE (blue line) and IVE+AgNPs (red line).

DISCUSSION

The biological synthesis of silver nanoparticles (AgNPs) using botanical extracts offers a green, cost-effective, and eco-friendly alternative to conventional physical and chemical routes. In the present study, aqueous extract of *Illicium verum* (star anise) served as a dual reducing and capping agent to form stable metallic AgNPs, which were comprehensively characterized and evaluated for their cytotoxic potency.

Synthesis Kinetics and Optical Confirmation, The immediate visual color transition upon mixing aqueous *I. verum* extract (IVE) with $AgNO_3$ solution, accompanied by a sharp Surface Plasmon Resonance (SPR) peak at approximately 420 nm, confirms the reduction of Ag^+ ions to Ag^0 nanoparticles. SPR arises from the collective oscillation of conduction band electrons on the nanoparticle surface when excited by incident light. Absorption maxima localized in the $410 - 440$ nm optical region are well-established benchmarks for spherical or quasi-spherical biogenic AgNPs. These spectral features align directly with findings reported for other spice-mediated syntheses, such as *Syzygium aromaticum* and *Cinnamomum verum*, where active polyphenolic constituents similarly drive rapid metal ion reduction.

Crystallographic Structure and Phyto-Capping Mechanisms, The structural and chemical stability of plant-synthesized AgNPs depend strongly on their crystal lattice and surface capping layer: XRD Phase Analysis: The distinct X-ray diffraction reflections at (111), (200), (220), and (311) confirm a pure, face-centered cubic (FCC) metallic lattice, matching standard JCPDS data (card no. 04-0783). Additional minor, unassigned reflections observed between $2\theta = 20°$ and $35°$ indicate the crystallization of surface-bound bio-organic compounds. Similar secondary diffraction features are widely documented in green synthesis literature and represent organic phytochemical shells coating the metallic core. FTIR Surface Functionalization: FTIR spectroscopy identified functional groups responsible for reduction and capping, showing major vibrational bands at $3420\ cm^{-1}$ (O–H/N–H stretching), $1640\ cm^{-1}$ (C=O Amide I / C=C aromatic stretching), and $1030\ cm^{-1}$ (C–O stretching). These bands correspond to bioactive constituents of *I. verum*, including trans-anethole, polyphenols, and soluble proteins. These phytocompounds reduce Ag^+ precursors while establishing a steric barrier that prevents nanoparticle aggregation.

In Vitro Antiproliferative Activity, The MTT assay demonstrated a clear dose-dependent reduction in cell viability across the concentration gradient ($0.15\ \mu$M/mL to $153.60\ \mu$M/mL). Cytotoxicity Profile: Low concentrations ($0.15 - 2.40\ \mu$M/mL) exhibited minimal impact on cell survival (>85%), whereas dosage near $19.20\ \mu$M/mL yielded $\sim 50\%$ inhibition (IC_{50}). Higher doses ($153.60\ \mu$M/mL) produced profound cell death (>85% mortality). Mechanism of Action: The heightened cytotoxic efficacy of biogenic AgNPs stems from their nanoscale dimensions and high surface area. Particle internalization via endocytosis triggers intracellular ion release, generation of reactive oxygen species (ROS), mitochondrial membrane depolarisation, and

activation of apoptotic pathways. The surface-adsorbed phytochemicals further act synergistically with the silver core to disrupt cell survival networks. (Figure 4)

CONCLUSION

In conclusion, this study successfully demonstrated the green, eco-friendly synthesis of silver nanoparticles (IVE-AgNPs) using the aqueous fruit extract of *Illicium verum* as a sustainable reducing and capping agent. UV–Vis spectroscopic analysis confirmed the formation of AgNPs, displaying a characteristic surface plasmon resonance (SPR) peak at approximately 420 nm. XRD characterization verified that the synthesized nanoparticles possess a highly crystalline, face-centered cubic (FCC) structure, while FTIR spectra confirmed the participation of plant-derived functional groups—including polyphenols, proteins, and flavonoids—in the bioreduction and capping process. Biological evaluation via the MTT assay revealed a clear dose-dependent cytotoxic effect for both IVE and IVE-AgNPs, with an estimated IC_{50} value around $19.20\ \mu$M/mL and severe toxicity observed at higher doses ($153.60\ \mu$M/mL). Overall, *I. verum*-mediated AgNPs present a promising, biogenic platform for biomedical applications and further therapeutic development.

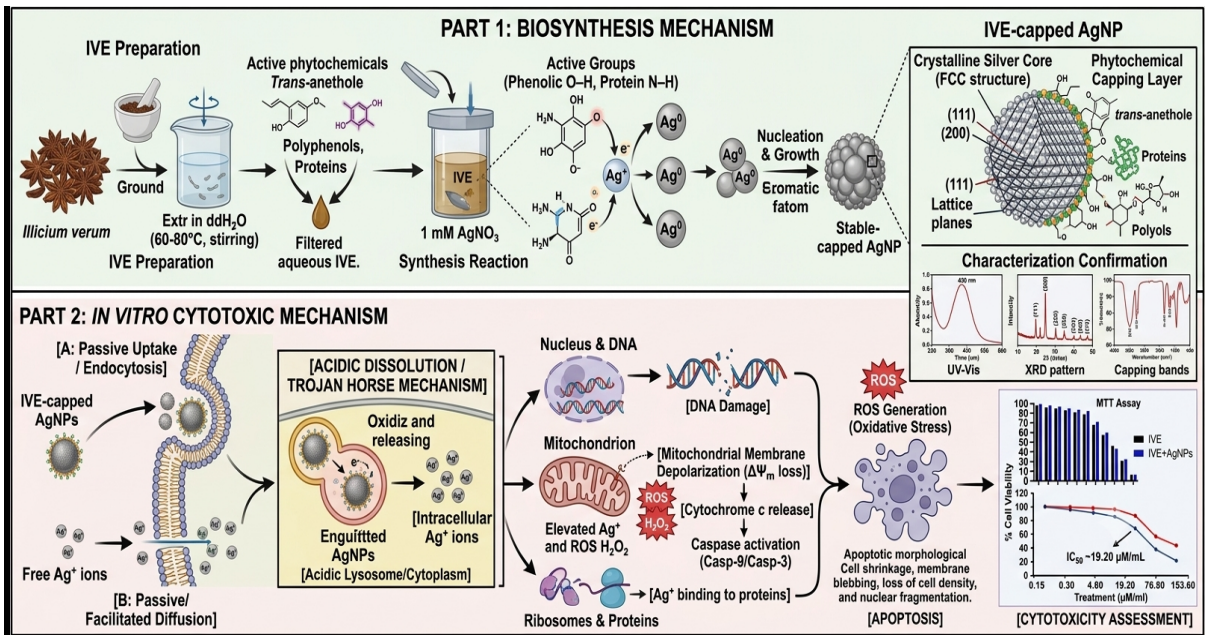

Figure 4. Schematic representation of *Illicium verum*-mediated silver nanoparticle (IVE-AgNP) synthesis, characterization, and cytotoxic mechanism. Aqueous *I. verum* fruit extract (IVE) rich in trans-anethole, polyphenols, and proteins facilitates the bioreduction of Ag^{+} ions to metallic Ag^{0}, yielding stable face-centered cubic (FCC) crystalline AgNPs capped by organic phytocompounds. Formation and surface capping are confirmed by UV-Vis (SPR ~ 420 nm), XRD, and FTIR analysis. Internalized IVE-AgNPs undergo intracellular oxidation in acidic endo/lysosomes, continuously releasing Ag^{+} ions via a "Trojan Horse" mechanism. The concurrent burst of reactive oxygen species (ROS) induces single/double-strand DNA damage, loss of mitochondrial membrane potential ($\Delta\Psi_m$), cytochrome *c* release, and caspase-9/3 cascade activation, leading to apoptotic cell death ($IC_{50} \approx 19.20\ \mu$M/mL).

REFERENCE

[1] Gurunathan S, Park JH, Han JW, Kim JH. Comparative assessment of the apoptotic potential of silver nanoparticles synthesized by *Bacillus tequilensis* and *Calocybe indica* in MDA-MB-231 human breast cancer cells: targeting p53 for anticancer therapy. Int J Nanomedicine. 2015;10:4203-4222. doi:10.2147/IJN.S83953.

[2] Sharafan M, Jafernik K, Ekiert H, Kubica P, Kocjan R, Blicharska E, Szopa A. *Illicium verum* (star anise) and trans-anethole as valuable raw materials for medicinal and cosmetic applications. Molecules. 2022;27(3):650. doi:10.3390/molecules27030650.

[3] Li WR, Xie XB, Shi QS, Zeng HY, Ou-Yang YS, Chen YB. Antibacterial activity and mechanism of silver nanoparticles on *Escherichia coli*. Appl Microbiol Biotechnol. 2010;85:1115-1122. doi:10.1007/s00253-009-2159-5.

[4] Mukherjee P, Ahmad A, Mandal D, Senapati S, Sainkar SR, Khan MI, et al. Fungus-mediated synthesis of silver nanoparticles and their immobilization in the mycelial matrix: a novel biological approach to nanoparticle synthesis. Nano Lett. 2001;1(10):515-519. doi:10.1021/nl0155274.

[5] Chernousova S, Epple M. Silver as antibacterial agent: ion, nanoparticle, and metal. Angew Chem Int Ed. 2013;52(6):1636-1653. doi:10.1002/anie.201205923.

[6] Li CY, Zhang YJ, Wang M, Zhang Y, Chen G, Li L, et al. In vivo real-time visualization of tissue blood flow and angiogenesis using Ag2S quantum dots in the NIR-II window. Biomaterials. 2014;35(2):393-400. doi:10.1016/j.biomaterials.2013.10.010.

[7] Sondi I, Salopek-Sondi B. Silver nanoparticles as antimicrobial agent: a case study on *Escherichia coli* as a model for Gram-negative bacteria. J Colloid Interface Sci. 2004;275(1):177-182. doi:10.1016/j.jcis.2004.02.012.

[8] Li L, Hu J, Yang W, Alivisatos AP. Band gap variation of size- and shape-controlled colloidal CdSe quantum rods. Nano Lett. 2001;1(7):349-351. doi:10.1021/nl015559r.

[9] Altammar KA. A review on nanoparticles: characteristics, synthesis, applications, and challenges. Front Microbiol. 2023;14:1155622. doi:10.3389/fmicb.2023.1155622.

[10] Fahim M, Shahzaib A, Nishat N, Jahan A, Bhat TA, Inam A. Green synthesis of silver nanoparticles: a comprehensive review of methods, influencing factors, and applications. JCIS Open. 2024;16:100125. doi:10.1016/j.jciso.2024.100125.

[11] Chaloupka K, Malam Y, Seifalian AM. Nanosilver as a new generation of nanoproduct in biomedical applications. Trends Biotechnol. 2010;28(11):580-588. doi:10.1016/j.tibtech.2010.07.006.

[12] McShan D, Ray PC, Yu H. Molecular toxicity mechanism of nanosilver. J Food Drug Anal. 2014;22(1):116-127. doi:10.1016/j.jfda.2014.01.010.

[13] Zhang J, Shi W, Ma Q, Cui H, Zhang L. Application of nanotechnology in immunity against infection. Coatings. 2021;11(4):430. doi:10.3390/coatings11040430.

[14] Malik S, Muhammad K, Waheed Y. Nanotechnology: a revolution in modern industry. Molecules. 2023;28:661.

[15] Assad N, Laila MB, Hassan MNU, et al. Eco-friendly synthesis of gold nanoparticles using *Equisetum diffusum* D. Don with broad-spectrum antibacterial, anticancer, antidiabetic, and antioxidant potentials. Sci Rep. 2025;15:1-16.

[16] Noor A, Ahmad N, Ali A, et al. Green synthesis of silver-doped ZnO nanoparticles from *Adiantum venustum* D. Don (Pteridaceae): antimicrobial and antioxidant evaluation. J Basic Microbiol. 2025. doi:10.1002/jobm.202400543.

[17] Gajanan K, Tijare SN. Applications of nanomaterials. Mater Today Proc. 2018;5:1093-1096.

[18] Gul H, Khan HA, Nasreen Z, et al. Exploring the antibacterial, anticoagulant, and hemolytic potential of green-synthesized Fe2O3 nanoparticles by *Cucurbita pepo* pulp. IEEE Trans Nanobiosci. 2025. doi:10.1109/TNB.2025.3563307.

[19] Mackeen MM, Ali AM, El-Sharkawy SH, et al. Antimicrobial and cytotoxic properties of some Malaysian traditional vegetables (Ulam). Int J Pharmacogn. 1997;35(3):174-178.

[20] Ali AM, El-Sharkawy SH, Hamid JA, Nur-Hediani I, Lajis NH. Antimicrobial activity of some Malaysian plants. Pertanika J Trop Agric Sci. 1995;18(1):49-52.

[21] Ali AM, Mackeen MM, El-Sharkawy SH. Antiviral and cytotoxic activities of some plants used in Malaysian indigenous medicine. Pertanika J Trop Agric Sci. 1996;19(2-3):129-136.